

TWO-DIMENSIONAL MODEL SEISMOLOGY*

JACK OLIVER,† FRANK PRESS,† AND MAURICE EWING†

ABSTRACT

The solutions of many problems in seismology may be obtained by means of ultrasonic pulses propagating in small scale models. Thin sheets, serving as two dimensional models, are particularly advantageous because of their low cost, availability, ease of fabrication into various configurations, lower energy requirements, and appropriate dilatational-to-shear-velocity ratios. Four examples are presented: flexural waves in a sheet, Rayleigh waves in a low velocity layer overlying a semi-infinite high velocity layer, Rayleigh waves in a high velocity layer overlying a semi-infinite low velocity layer, and body and surface waves in a disk.

INTRODUCTION

In recent years investigators in both the commercial and academic fields have attacked the problems of elastic wave propagation by studying waves of ultrasonic frequencies traveling through small scale three-dimensional models, and a few papers have been published on the subject (Kaufman and Roever, 1951; Northwood and Anderson, 1953; Terada and Tsuboi, 1927). Although promising results were obtained, widespread application of the method to significant problems has been slow, chiefly because of the difficulties in procuring suitable model materials and in the fabrication of desirable configurations. This paper describes the use of two-dimensional models, which virtually eliminates these and other difficulties without detracting from the usefulness of the method in a great majority of cases.

The models take the form of thin sheets and the propagation takes place along directions lying in the plane of the sheet. In practice these sheets are generally 1/16 inch thick, and only wavelengths long compared to this thickness are employed.

THEORY

We wish to determine the velocities of propagation of dilatational and shear waves in a thin plate and of Rayleigh waves on the edge of a thin plate. We restrict ourselves to waves in which the particle motion is symmetrical about the median plane of the plate, thus excluding any type of wave motion which involves bending of the thin plate.

Love's concept of a "generalized plane stress" (Love, 1944) is applicable and most convenient. The x and y directions are taken in the plane of the plate, the z direction perpendicular to it. X_y is the stress in the x direction on the face normal to the y axis, etc. Love's concept supposes the stress Z_z to vanish throughout the plate and the tangential stress Z_x and Y_z to vanish at $z = \pm h/2$ only,

* Manuscript received by the Editor December 7, 1953.

† Lamont Geological Observatory, Columbia University, Palisades, N. Y.

where h is the plate thickness. For a thin plate, Love takes average values of the components of displacement, strain and stress, e.g.

$$\bar{u} = \frac{1}{h} \int_{-h/2}^{h/2} u dz.$$

u and v are the displacements in the x and y directions respectively.

In the following we use only average values for these quantities and the bar is omitted.

The equations of motion are

$$\frac{\partial X_x}{\partial x} + \frac{\partial X_y}{\partial y} = \rho \frac{\partial^2 u}{\partial t^2}, \quad \frac{\partial Y_x}{\partial x} + \frac{\partial Y_y}{\partial y} = \rho \frac{\partial^2 v}{\partial t^2} \quad (1)$$

where ρ is the density.

The average stress components are given by Love as

$$X_x = \frac{2\lambda\mu}{\lambda + 2\mu} \left(\frac{\partial u}{\partial x} + \frac{\partial v}{\partial y} \right) + 2\mu \frac{\partial u}{\partial x} \quad (2a)$$

$$Y_y = \frac{2\lambda\mu}{\lambda + 2\mu} \left(\frac{\partial u}{\partial x} + \frac{\partial v}{\partial y} \right) + 2\mu \frac{\partial v}{\partial y} \quad (2b)$$

$$X_y = \mu \left(\frac{\partial v}{\partial x} + \frac{\partial u}{\partial y} \right). \quad (2c)$$

Substituting (2) into (1),

$$\rho \frac{\partial^2 u}{\partial t^2} = \left(\frac{2\mu\lambda}{\lambda + 2\mu} + \mu \right) \frac{\partial \tau}{\partial x} + \mu D^2 u \quad (3)$$

and similarly in v , where

$$\tau = \frac{\partial u}{\partial x} + \frac{\partial v}{\partial y} \quad \text{and} \quad D^2 = \frac{\partial^2}{\partial x^2} + \frac{\partial^2}{\partial y^2}.$$

Differentiate equation (3) with respect to x and the similar equation in v with respect to y and add the results to obtain

$$\rho \frac{\partial^2 \tau}{\partial t^2} = \frac{4\mu(\lambda + \mu)}{\lambda + 2\mu} D^2 \tau. \quad (4)$$

Equation (4) checks the velocity given by Lamb for dilatational waves in a thin plate, i.e.

$$V_p = \left[\frac{4\mu(\lambda + \mu)}{\rho(\lambda + 2\mu)} \right]^{1/2}. \quad (5)$$

Take the curl (two dimensional) of equation (3) to obtain

$$\rho \frac{\partial^2}{\partial t^2} \left(\frac{\partial u}{\partial y} - \frac{\partial v}{\partial x} \right) = \mu D^2 \left(\frac{\partial u}{\partial y} - \frac{\partial v}{\partial x} \right). \quad (6)$$

Thus the shear wave velocity is the same as in an infinite solid, i.e.

$$\beta = \left(\frac{\mu}{\rho} \right)^{1/2}.$$

We now consider a thin plate which occupies the xy plane from $y=0$ to $y=+\infty$. Let

$$u = \frac{\partial \phi}{\partial x} + \frac{\partial \psi}{\partial y}, \quad v = \frac{\partial \phi}{\partial y} - \frac{\partial \psi}{\partial x}; \quad (7)$$

then

$$D^2 \phi = \tau, \quad D^2 \psi = \frac{\partial u}{\partial y} - \frac{\partial v}{\partial x}$$

where ϕ and ψ satisfy

$$\frac{\partial^2 \phi}{\partial t^2} = V_p^2 D^2 \phi, \quad \frac{\partial^2 \psi}{\partial t^2} = \beta^2 D^2 \psi. \quad (8)$$

Choose plane wave solutions of the form

$$\begin{aligned} \phi &= A e^{i k (-r y + x - c t)} \\ \psi &= B e^{i k (-s y + x - c t)} \end{aligned} \quad (9a)$$

where

$$r = \left(\frac{c^2}{V_p^2} - 1 \right)^{1/2}, \quad s = \left(\frac{c^2}{\beta^2} - 1 \right)^{1/2}. \quad (9b)$$

c is the velocity of propagation of constant phase in the x direction and k the wave number. Thus the wavelength in the x direction, l , is given by $l = 2\pi/k$ and the period T by $T = 2\pi/kc$.

At the free edge $y=0$,

$$X_y = Y_y = 0. \quad (10)$$

Using equation (2), (7), (9), and (10) we get

$$[V_p^2(1 + r^2) - 2\beta^2]A + 2\beta^2 s B = 0 \quad (11)$$

$$2rA + (1 - s^2)B = 0. \quad (12)$$

Eliminating A and B from (11) and (12) and using (9b)

$$\left(2 - \frac{c^2}{\beta^2}\right)^2 = 4 \left(1 - \frac{c^2}{V_p^2}\right)^{1/2} \left(1 - \frac{c^2}{\beta^2}\right)^{1/2} \quad (13)$$

This is identical with the equation for Rayleigh waves on the surface of a semi-infinite solid (Bullen, 1947) with the exception that the plate dilatational velocity replaces the infinite solid dilatational velocity. It is clear that no difficulties will arise in more complicated cases. Thus most of the problems on propagation of plane waves in a stratified earth may be related to the two dimensional models simply by replacing α by V_p .

EQUIPMENT AND TECHNIQUES

The principal features of the apparatus and procedure are described here briefly. The transmitting and receiving equipment is adapted from similar equipment in use in several laboratories, but the use of thin plates for construction of the models is apparently novel.

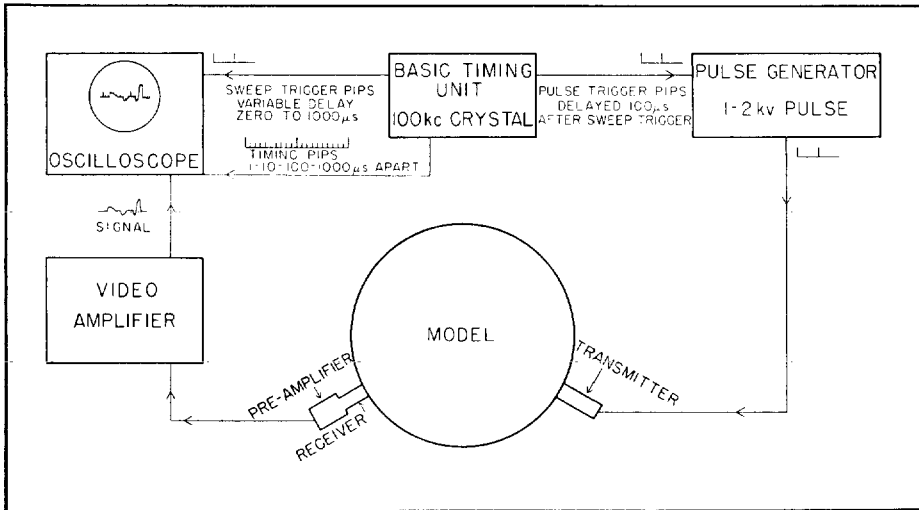


FIG. 1. Block diagram of apparatus.

A block diagram of the equipment is shown in Figure 1. Electrical pulses of approximately 15 microsecond duration are applied to the transmitter, a small piezoelectric element in contact with the model. This transducer delivers an acoustical pulse, shown as traced from the seismogram in Figure 2, to the model. The resulting acoustical energy arriving at various points on the model is detected by a similar transducer, amplified, and then displayed on the cathode ray oscilloscope. The pulse repetition rate is adjustable from 2 to 100 pulses per second. The oscilloscope sweep is triggered at a fixed time interval ahead of the pulse so that a standing wave pattern, including the time break, is observed. The basic

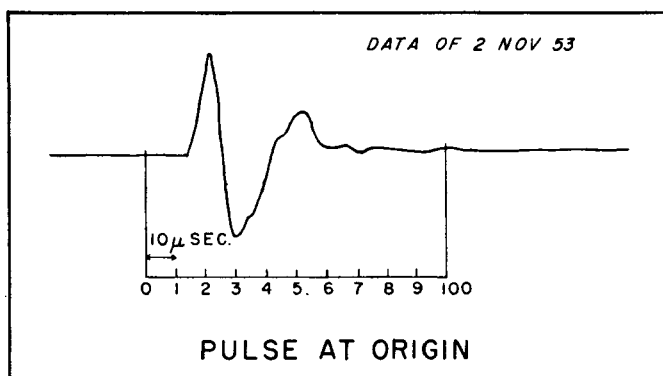


FIG. 2. Pulse at origin.

timing unit which initiates the trigger pulses for both the oscilloscope and the pulse also supplies timing markers at convenient intervals. The resulting pattern on the oscilloscope is then photographed by a Polaroid Land camera and the miniature seismogram is obtained immediately.

The transmitting transducer is a barium titanate cylinder $1/10$ inch thick and $\frac{1}{4}$ inch in diameter. To prevent internal reflections in the source mount, the transducer is backed by a long aluminum rod of the same diameter. The part of the energy that enters the backing and then reflects from the end of the rod back toward the source is too late and too greatly attenuated to confuse the seismogram. Difficulties due to free oscillations or "ringing" of the source are avoided by utilizing a frequency range that is below the ringing frequency of the transducer. The receiving transducer is also of barium titanate $1/25$ inch thick and $3/32$ inch in diameter and is mounted in a similar but less elaborate manner. The smaller thickness further improves the reduction of ringing.

The electronic equipment is currently being improved and will be thoroughly described in a later report. The present unit delivers a pulse of about 1,000–2,000 volts to the source crystal. The voltage amplification of the receiving unit is less than 100,000.

The two-dimensional models are usually built in the form of disks. These are particularly advantageous for the study of surface waves on the edge of the disk since there are no reflections of the surface waves and since a very long path may be obtained by using the multiple trips around a relatively small disk. The curvature of the disk may be made small compared to a wavelength so that the usual surface wave equations for flat-lying strata will be applicable with the slight modification of the dilatational wave velocity, or it may be made larger for studying the effect of sphericity of the earth upon long period surface waves. The body phases of earthquake seismology may be studied in the usual manner very conveniently. Any degree of complexity in the layering may be obtained by means of concentric rings of various materials glued together in the desired rela-

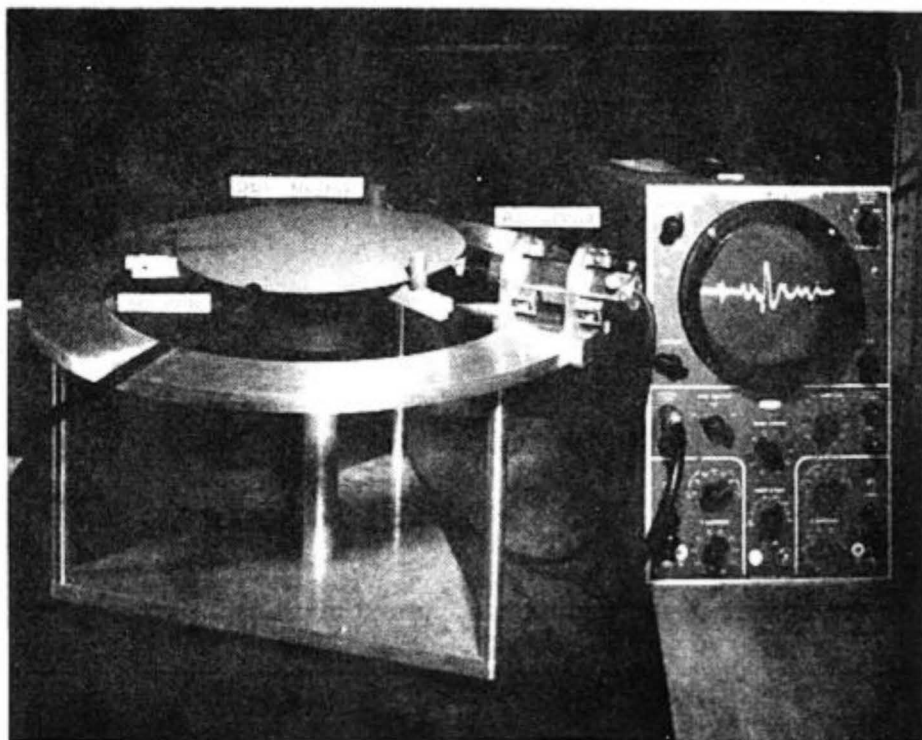


FIG. 3. Model, transducers, and oscilloscope.

tion. The diameters of the disks used in this study are about 20 inches. The thickness is at present standardized at $1/16$ inch. This is small compared to all the wavelengths involved so that there is no dispersion due to finite disk thickness. For some types of problems shapes other than the circular might be desirable; e.g., refraction and reflection problems of seismic prospecting may be studied by constructing a cross section of the configuration in question. Table 1 lists the materials that have been sampled to date with the compressional, shear and Rayleigh velocities.

The disks are held in position by three rubber-covered supports which touch them at three points on the periphery (Figure 3). Experiments show that for a disk of this thickness the supports do not affect the surface wave propagation appreciably. The disk is mounted concentric with a graduated ring on which the receiver travels, allowing accurate measurement of all arc distances. The transmitting transducer is set at an arbitrary zero which may be determined accurately by running profiles from the transducer in both directions. A plot of the dilatational wave travel times vs. distance immediately gives the zero of the transmitted pulse in both time and distance.

COMPARISON OF TWO- AND THREE-DIMENSIONAL MODELS

Two-dimensional models (2-D) have the following advantages over three-dimensional (3-D) models.

1. The materials are far less expensive. 3-D models are usually constructed of some material which can be poured, e.g., wax, concrete, tars, or various chemical setting cements, or of some material which can be purchased in large slabs, e.g., limestone, marble, etc. All of these are expensive and become increasingly difficult to handle when layered media are desired. It is particularly difficult to pour materials in large blocks and maintain homogeneity throughout. The 2-D models, on the other hand, may be constructed of any material which can be bought in 1/16 inch sheets. This includes most metals and alloys and many types of plastics, fibers, etc. They are not prohibitively expensive and are generally far more homogeneous than poured materials.

2. The fabrication is greatly simplified. Layered configurations may be built up from concentric rings, easily cut to accurate specifications on a large lathe. Almost any sort of hard glue may be used as a binding agent.

3. Storage is simplified, a drawer of a map case may be used for storage of a large number of 2-D models. 3-D models frequently require about 50 sq ft of floor space for each model.

4. The energy requirements are greatly diminished in the 2-D model. For body waves the intensity varies as $1/R$, as opposed to $1/R^2$ in the 3-D case. Surface waves undergo no geometrical attenuation, instead of the $1/R$ variation in the 3-D case. This is a tremendous advantage as it allows the use of pulses of 1,000 volts or less as opposed to 5,000–10,000 volts in the 3-D case. Similarly lower gains may be used in the amplifying system, which permits use of a simple receiving circuit.

5. Most materials commercially available do not make good models of rock because Poisson's ratio is too large, usually about 0.33 as opposed to about 0.25 for rocks. In the 2-D model the dilatational wave velocity is altered (see theory) so that a pseudo-Poisson's ratio (the same relation of the dilatational and shear velocities as for Poisson's ratio) now falls in the range appropriate to rocks (see Table 1).

6. Multiple trips around the disk by the surface waves may be used to give large path distances. The present paper includes waves that have made $2\frac{1}{2}$ trips (about 13 feet) but waves have been observed that have made $7\frac{1}{2}$ complete circuits (about 40 feet). Although a similar scheme might be followed three-dimensionally by using a sphere, the construction of spheres, particularly with concentric layers, is very difficult.

The multiple paths also provide a means of measuring attenuation that is free of instrument calibration and differences in coupling of the model to the transducer. This approach is identical to that used in the measurement of the absorption coefficient of the mantle by means of long Rayleigh waves (Ewing and Press, in press).

TABLE I
MEASURED ELASTIC WAVE VELOCITIES AND DENSITIES

Material	Designation	Sample	Plate Dilatation Velocity V_p in ft/sec	Shear Velocity, β in ft/sec	Rayleigh Velocity, V_r in ft/sec	Density ρ in gm/cc	Pseudo- Poisson's Ratio: $\frac{1}{2} - (\beta/V_p)^2$	Remarks
							$\frac{1}{1 - (\beta/V_p)^2}$	
Aluminum	24S-T4	Disk	18,300	10,400	9,800	2.77	.26	
Alloy		$\frac{1}{16}'' \times 10.56''$						
Plexiglass	Colorless, Trans- parent	Disk	7,750	4,500	4,200	1.22	.25	
		$\frac{1}{16}'' \times 10.75''$						
Panelyte	Grade 550	Disk	10,650	6,000	5,600	1.44	.27	Anisotropic* 2%
		$\frac{1}{16}'' \times 19.522''$						
Copper	Cold rolled	$\frac{1}{16}'' \times 10.75''$	13,000	7,500	6,900	9.03	.25	
Steel	Cold rolled	$\frac{1}{16}'' \times 10.75''$	17,850	10,650	9,700	7.78	.22	
Steel	Hot rolled	$\frac{1}{16}'' \times 10.75''$	17,600	10,300	9,700	7.80	.24	
Brass	Half hard	$\frac{1}{16}'' \times 10.75''$	12,500	7,000	6,500	8.34	.28	
Zinc		.052" $\times 10.75''$	13,100	7,700	7,300	7.07	.24	
Vinyl Plastic	Phonograph record	$\frac{1}{16}'' \times 11.875''$	6,420	3,870	3,540	1.47	.21	
Fish paper	Franklin Fibre	$\frac{1}{16}'' \times 10.875''$	8,970	5,490	5,110	1.14	.22	Anisotropic* 22%
	Lamitex							
Fibre	Franklin Hard	$\frac{1}{16}'' \times 10.875''$	8,650	5,270	4,900	1.06	.21	Anisotropic* 15%
	Vulcanized							
Formica	Linen Laminate	$\frac{1}{16}'' \times 10.75''$	8,450	5,050	4,700	1.30	.24	Anisotropic* 7%

* For anisotropic materials slowest velocities are tabulated. These are generally perpendicular to the grain. For Panelyte the tabulated velocity is an average.

At present 3-D models are necessary only when one or more layers of a stratified configuration is a liquid or when it is desirable to model three-dimensional effects such as reflections not in the vertical plane of the shot and detector, which might be encountered in seismic prospecting.

EXAMPLES

Flexural Waves

The experimental model for studying the propagation of flexural waves in a plate, as worked out by Lamb (1917), was a ring cut from 24 ST Aluminum sheet, 1/16 inch thick. The outside diameter $2R_2$ of the ring was 19.112 inches and the inside diameter $2R_1$, $\frac{1}{2}$ inch less. Radial motions of the ring were investigated as the 2-D analog of ordinary flexural waves. Figure 4 is a tracing of the oscillogram obtained with the receiver at the antipodes of the source. At this point there is constructive interference between the waves arriving from opposite directions. The first arrival following the time break corresponds to a dilatational wave through the ring. The first dispersive train of flexural waves corresponds to R_1 and R_2 , the second to R_3 and R_4 , etc., where the R 's with subscripts are used in the same sense as in earthquake seismology. The values obtained from the experimental data are plotted as the small circles of Figure 5.

The theoretical equations for wave motion in an elastic plate in a vacuum were presented by Lamb (1917). The dispersion of flexural waves is determined by his period equation for asymmetrical motion. In our notation this equation takes the form

$$\frac{\tanh \frac{kh}{2} \left(1 - \frac{c^2}{\beta^2}\right)^{1/2}}{\tanh \frac{kh}{2} \left(1 - \frac{c^2}{\alpha^2}\right)^{1/2}} = \frac{\left(2 - \frac{c^2}{\beta^2}\right)^2}{4 \left(1 - \frac{c^2}{\alpha^2}\right)^{1/2} \left(1 - \frac{c^2}{\beta^2}\right)^{1/2}} \quad (14)$$

where h is the layer thickness.

To adapt this to our 2-D models we need only replace α by V_p and h by $R_2 - R_1 \equiv H$. Group velocity is obtained from the well known formula

$$U = c + \kappa H \frac{\partial c}{\partial(kH)} \quad (15)$$

A family of theoretical curves of group velocity vs. period computed with the constants for 24 ST Aluminum alloy is shown in Figure 5. Thickness is the parameter and very close agreement with the observed points is evident. Thus we have a good check on both the theory and the experimental method.

Slight complications have arisen due to the shape of the source pulse, in particular the later origin times of the longer periods. This difficulty may be completely circumvented by measuring arrival times of each period on successive

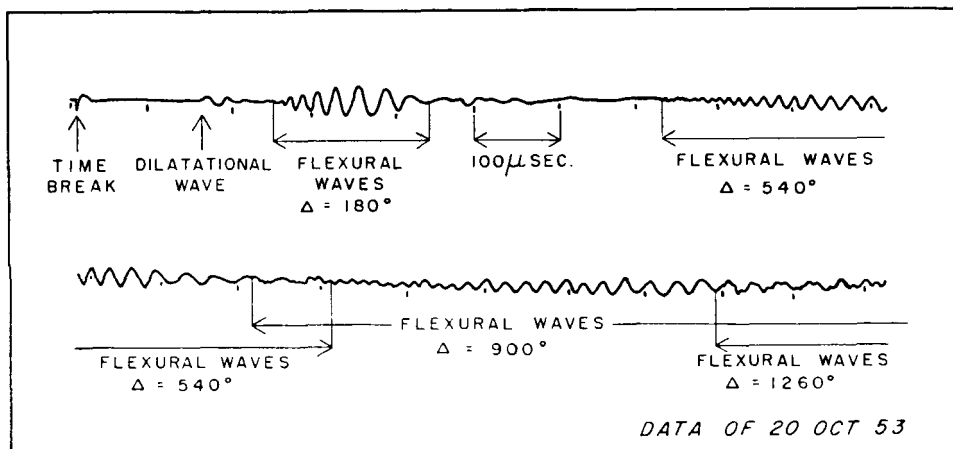


FIG. 4. Seismogram—flexural waves.

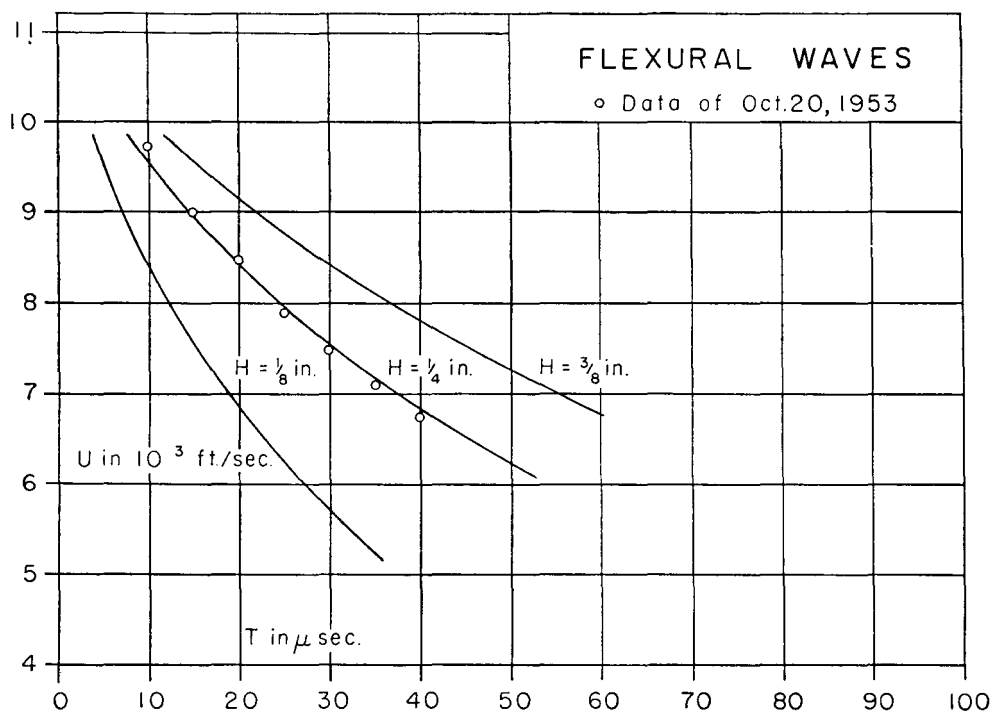


FIG. 5. Flexural wave dispersion.

trips around the ring and calculating the group velocity over the interval. The points of Figure 5 were obtained by this method. If the initial rise of the source is used as a time break, a maximum error of 2% in the velocity might result. This effect is interesting and will be the subject of future study but it does not affect the present results.

Rayleigh Waves—Low Velocity over High Velocity

The most common configuration in nature which produces dispersion in Rayleigh waves is comprised of a low velocity layer of thickness h over a high velocity semi-infinite layer. Lee (1932) has presented the theoretical equations for this case. His period equation is

$$\xi\eta' = \xi'\eta \quad (16)$$

where

$$\begin{aligned} \xi &= \left(2 - \frac{c^2}{\beta^2}\right) \left[\left(\frac{c^2}{\beta'^2} \frac{\mu'}{\mu} - \phi \right) \cos kh\eta_1 + \frac{\eta_1'}{\eta_1} \left(\frac{c^2}{\beta^2} + \phi \right) \sin kh\eta_1 \right] \\ &\quad + 2\eta_2 \left[\eta_1' \phi \sin kh\eta_2 - \frac{1}{\eta_2} \left(\frac{c^2}{\beta'^2} \frac{\mu'}{\mu} - \phi - \frac{c^2}{\beta^2} \right) \cos kh\eta_2 \right] \\ \xi' &= \left(2 - \frac{c^2}{\beta^2}\right) \left[\eta_2' \phi \cos kh\eta_1 + \frac{1}{\eta_1} \left(\frac{c^2}{\beta'^2} \frac{\mu'}{\mu} - \phi - \frac{c^2}{\beta^2} \right) \sin kh\eta_1 \right] \\ &\quad + 2\eta_2 \left[\left(\frac{c^2}{\beta'^2} \frac{\mu'}{\mu} - \phi \right) \sin kh\eta_2 - \frac{\eta_2'}{\eta_2} \left(\frac{c^2}{\beta^2} + \phi \right) \cos kh\eta_2 \right] \\ \eta &= \left(2 - \frac{c^2}{\beta^2}\right) \left[\eta_1' \phi \cos kh\eta_2 - \frac{1}{\eta_2} \left(\frac{c^2}{\beta'^2} \frac{\mu'}{\mu} - \phi - \frac{c^2}{\beta^2} \right) \sin kh\eta_2 \right] \\ &\quad + 2\eta_1 \left[\left(\frac{c^2}{\beta'^2} \frac{\mu'}{\mu} - \phi \right) \sin kh\eta_1 - \frac{\eta_1'}{\eta_1} \left(\frac{c^2}{\beta^2} + \phi \right) \cos kh\eta_1 \right] \\ \eta' &= \left(2 - \frac{c^2}{\beta^2}\right) \left[\left(\frac{c^2}{\beta'^2} \frac{\mu'}{\mu} - \phi \right) \cos kh\eta_2 + \frac{\eta_2'}{\eta_2} \left(\frac{c^2}{\beta^2} + \phi \right) \sin kh\eta_2 \right] \\ &\quad + 2\eta_1 \left[\eta_2' \phi \sin kh\eta_1 - \frac{1}{\eta_1} \left(\frac{c^2}{\beta'^2} \frac{\mu'}{\mu} - \phi - \frac{c^2}{\beta^2} \right) \cos kh\eta_1 \right], \end{aligned}$$

and where

$$\phi = 2 \left(\frac{\mu'}{\mu} - 1 \right)$$

and

$$\eta_1 = \left(\frac{c^2}{\alpha^2} - 1 \right)^{1/2}, \quad \eta_2 = \left(\frac{c^2}{\beta^2} - 1 \right)^{1/2}$$

$$\eta_1' = \left(1 - \frac{c^2}{\alpha'^2} \right)^{1/2}, \quad \eta_2' = \left(1 - \frac{c^2}{\beta'^2} \right)^{1/2}$$

and the other symbols have the same meaning as before. Again we replace the α by V_p and the theoretical curves are shown in Figure 6. The computed points are tabulated in Table II. The constants were chosen to fit the case of Plexiglass overlying Panelyte. (See Table I.)

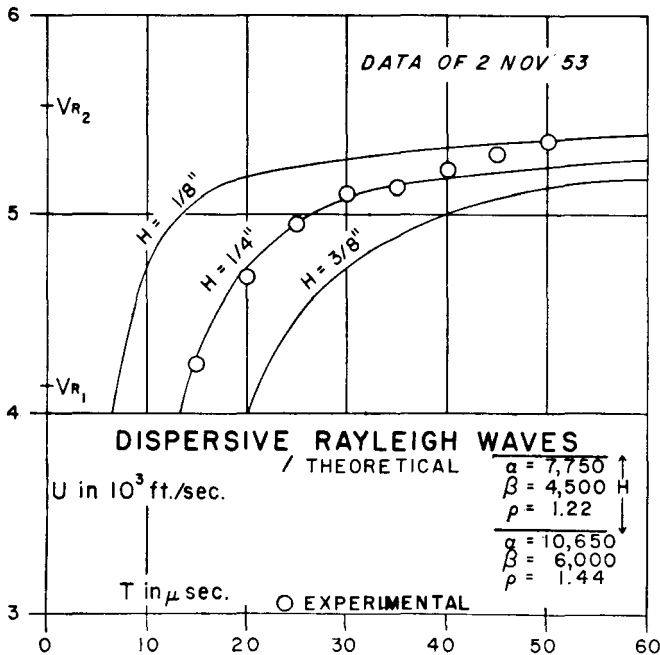


FIG. 6. Rayleigh wave dispersion—low velocity layer/high velocity substratum.

The disk was 19.522 inches in diameter with outside diameter of the outer ring $\frac{1}{2}$ inch greater. Figure 7 is a record taken at $\Delta = 180^\circ$. Because of the small contrast between these two materials and the high attenuation in the plastic, more precision was obtained by using seismograms at several different Δ 's rather than the one from the antipodes alone. As before, this eliminates the difficulty with the origin time of various periods in the pulse by making the velocity determination independent of pulse time. Figure 6 shows the experimental results in good agreement with the theory.

TABLE II

PHASE AND GROUP VELOCITY VS kH FOR A LAYER WITH $\alpha = 7,750$ FT/SEC, $\beta = 4,500$ FT/SEC,
 $\rho = 1.219$ GM/CC OVERLYING A SEMI-INFINITE LAYER WITH
 $\alpha = 10,650$ FT/SEC, $\beta = 6,000$ FT/SEC, $\rho = 1.436$

Computed values		Values obtained graphically		
c in ft/sec	kH	kH	U in ft/sec	c in ft/sec
5,535	0	0	5,535	5,535
5,500	.075	.05	5,488	5,510
5,450	.203	.1	5,449	5,490
5,400	.358	.2	5,379	5,453
5,330	.550	.3	5,323	5,418
5,300	.765	.4	5,276	5,388
5,200	1.152	.5	5,233	5,362
5,100	1.450	.75	5,123	5,302
5,000	1.722	1.00	4,987	5,241
4,900	1.955	1.25	4,766	5,168
4,800	2.196	1.50	4,543	5,083
4,700	2.425	1.75	4,283	4,977
4,600	2.689	2.00	4,020	4,838
4,400	3.392	2.25	3,842	4,973
4,300	3.965	2.50	3,685	4,672
4,200	5.107	2.90	3,623	4,528
		3.0	3,626	4,498
		4.0	3,770	4,296
		5.0	3,886	4,207

The Panelyte is anisotropic, having a velocity about $1\frac{1}{2}\%$ higher in one direction than in the perpendicular direction. This was not taken into account in the calculations and is a source of error in the comparison with the theoretical curves. The points for the two longest periods both fall high. These long periods can only be distinguished in the dispersive train after a considerable length of path has been traversed. At that time the amplitudes are low and, in fact, the relative am-

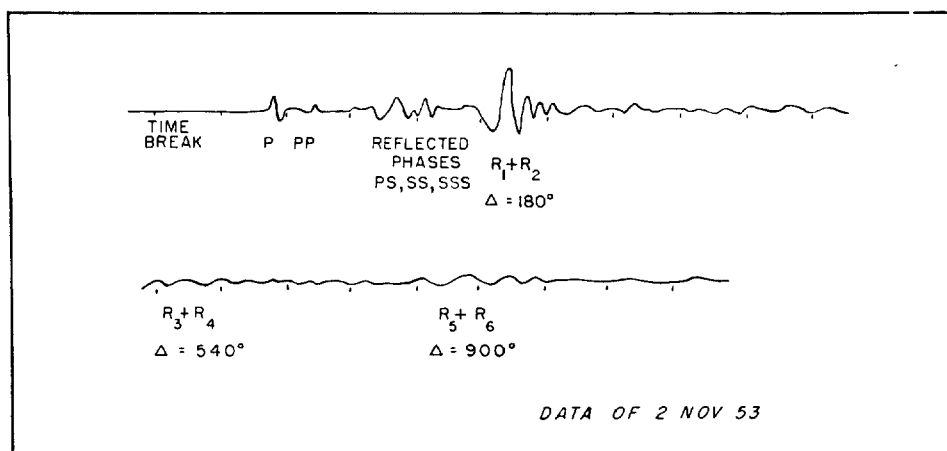


FIG. 7. Seismogram—low velocity layer/high velocity substratum.

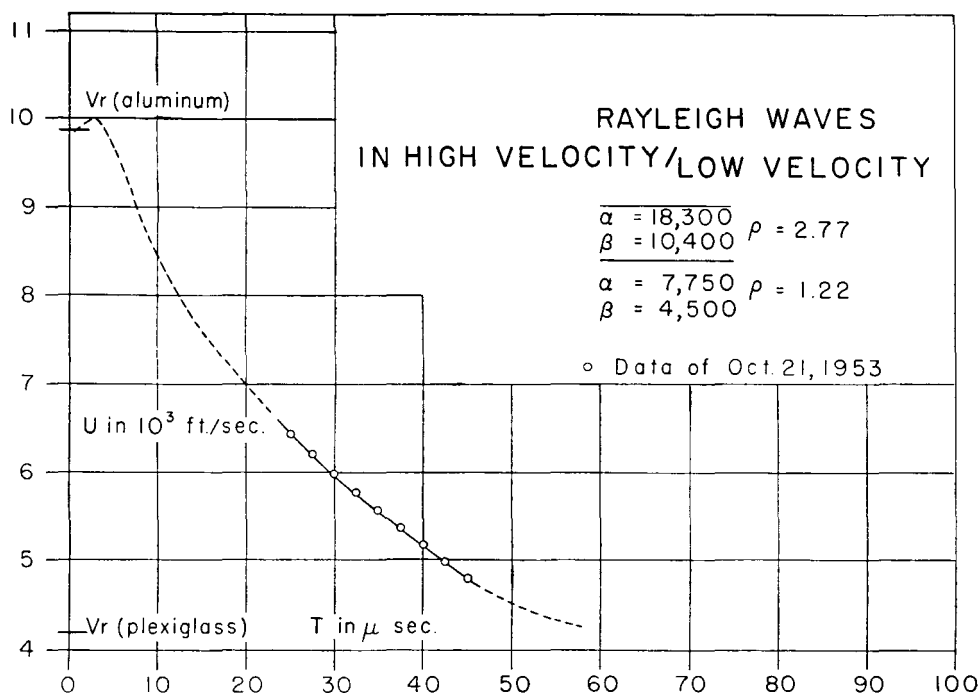


FIG. 8. Rayleigh wave dispersion—high velocity layer/low velocity substratum.

plitudes of such periods are always low due to the pulse shape. Thus the accuracy of velocity measurement is reduced for these waves. Furthermore, it is possible that these waves may be long enough to be affected by the curvature of the disk. The discrepancy is in the proper direction, but this effect has not yet been studied. At most, however, the error is 2%.

Experiments in higher mode Rayleigh waves (shear modes) and on Stoneley waves are planned.

Rayleigh Waves—High Velocity over Low Velocity

The previous examples have shown a comparison of experimental data with theoretical curves. In both cases the theoretical calculations were relatively simple and within the range of an ordinary desk calculator. In the case of a high velocity layer over a semi-infinite low velocity stratum the computations increase greatly in complexity. On the other hand, there is no difficulty in modelling this case. Figure 8 is a plot of the Rayleigh wave dispersion for the case of a ring of aluminum alloy overlying a disk of Plexiglass. Figure 9 is a tracing of the seismogram at the antipodes. The ring of aluminum is the same as that use for the flexural waves. This configuration corresponds to a layer of rock with elastic constants $\alpha = 18,300$ ft/sec and $\beta = 10,400$ ft/sec, overlying a semi-infinite layer with

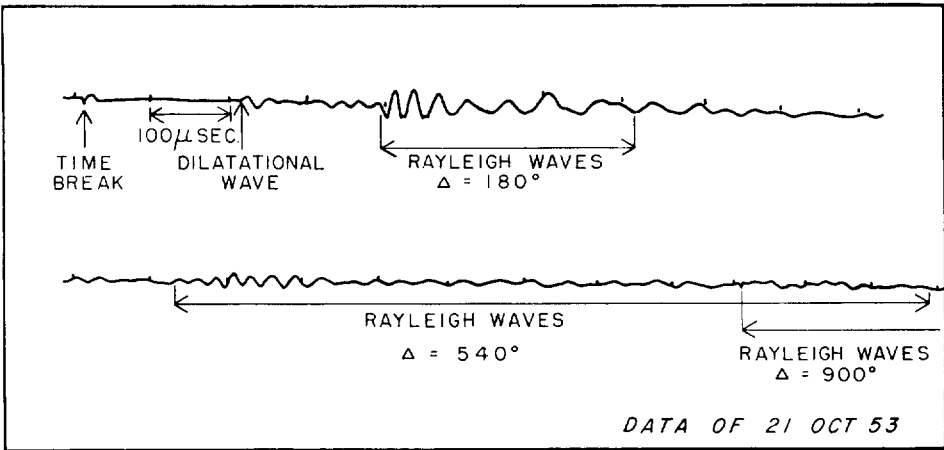


FIG. 9. Seismogram—high velocity layer/low velocity substratum.

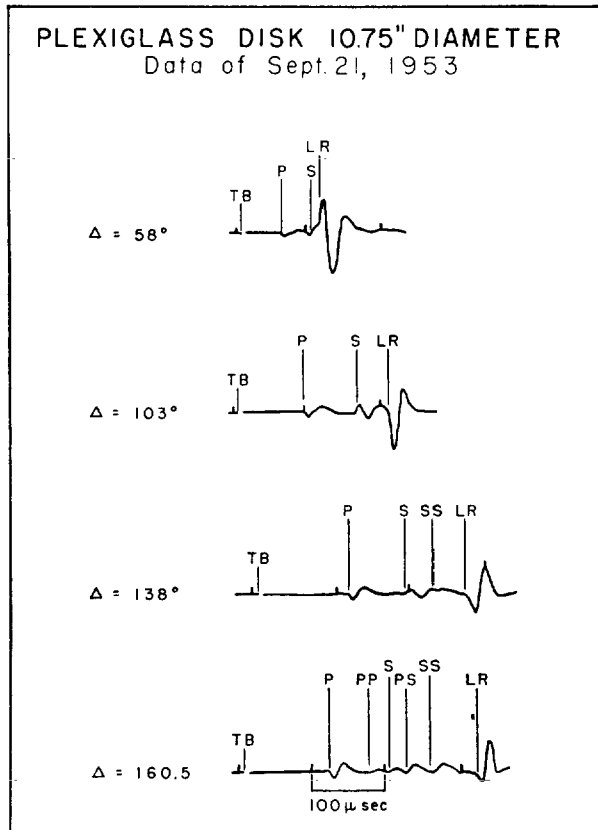


FIG. 10. Seismogram—Plexiglass disk.

$\alpha = 7,750$ ft/sec, $\beta = 4,500$ ft/sec. The ratio of the densities is $\rho/\rho' = 2.77/1.22$. This is a fair approximation to the case of Palisades diabase overlying Triassic sandstones and shales along the west bank of the Hudson River. It is also similar to structure in the permafrost areas in the Arctic.

Because of the limited spectrum of the pulse only a portion of the complete dispersion curve is obtained. Other segments may be studied by varying the thickness of the layer.

Body and Surface Waves in Disks

The previous examples, all concerning surface waves, used wavelengths which were small enough compared to the curvature of the disks so that the waves were effectively traveling along flat surfaces. Disks were chosen merely as a

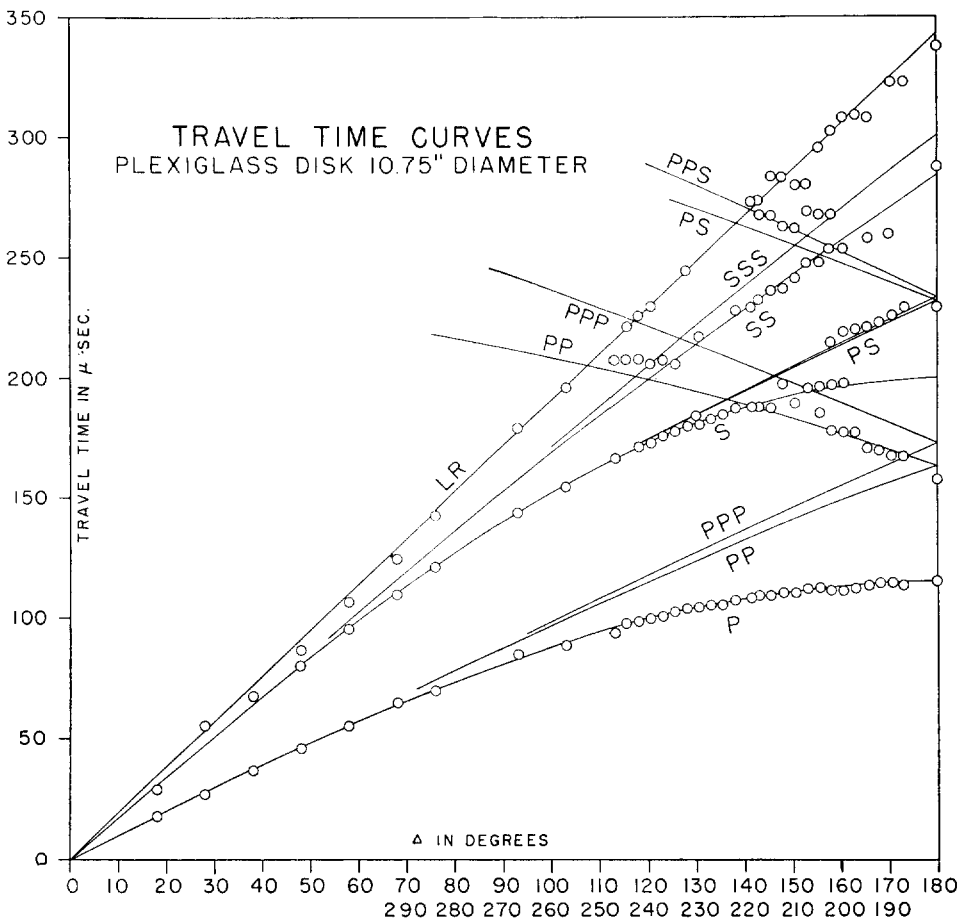


FIG. 11. Travel time curves—body and surface waves in a disk.

convenient shape to work with because of the multiple paths and lack of surface wave reflections. However the disk as a two-dimensional model of the earth also appears promising for the study of body waves. The seismograms of Figure 10 were taken on a uniform Plexiglass disk of diameter 10.75 inches. Figure 11 is a plot of the experimental points read from the records, compared with theoretical travel time curves based on velocities determined from the P arrivals. Poisson's ratio is taken as $\frac{1}{4}$. Phases definitely identifiable are P , PP , S , PS and PPS , SS , and LR . At the larger Δ 's there is some difficulty in determining the exact arrival time and phase of the later arrivals due to overlapping of other phases. The present picks for the later arrivals are nearly always late. Clearly, this can be avoided by the use of larger disks and future studies will be made on disks of at least twice this diameter. This should improve the resolution of phases and accuracy of the arrival times measurably.

The polarity of the first break of the Rayleigh wave changes with distance. Such is not the case for Rayleigh waves propagating along the straight edge of a plate, which rules out the possibility of selective absorption of the high frequencies as the cause. The change of polarity is possibly the result of the generation of the waves by the curved P and S wave fronts at the surface. The phenomenon is not understood at present.

Scaling to Related Problems

The dispersion curves of the preceding examples are presented in the dimensions as modeled. Scaling to other problems is a relatively simple matter, as can be seen from an inspection of the period equation for flexural waves or Rayleigh waves. Once a fixed relation is established between all the dilatational and shear velocities the equations may be solved for the ratio c/β or c/α and similarly U/β or U/α . Thus velocities may be scaled to any other problem for which the elastic constants have the same ratios merely by multiplying the measured velocities by the appropriate ratio β'/β or α'/α . Similarly, the period associated with a given phase and group velocity will vary directly with H , the layer thickness.

ACKNOWLEDGMENTS

The authors wish to acknowledge the assistance of many co-workers at the Lamont Geological Observatory. In particular, Mr. Charles Kershaw constructed all the electronic gear and designed the new components. Mr. James Dorman and Mr. Donald Schiller carried out the computations, and Mr. Louis Collyer built the mechanical parts of the apparatus. Mr. Paul Pomeroy made many of the velocity determinations.

The Carter Oil Company generously gave assistance in the design of circuits used, through Dr. Franklyn Levin, who participated in the seismic model work for that company.

REFERENCES

- Bullen, K. E., 1947, *An introduction to the theory of seismology*: Cambridge University Press.
- Ewing, M. and Press, Frank. *An investigation of mantle Rayleigh waves*: in press, *Bull. Seis. Soc. Am.*
- Kaufman, S. and Roever, W. L., 1951, *Laboratory studies of transient elastic waves*: The Hague, *Proceedings of Third World Petroleum Congress, Section I*, p. 537-545.
- Lamb, H., 1917, *On waves in an elastic plate*: *Proc. Roy. Soc. Lond. A* 93, p. 114.
- Lee, A. W., 1932, *The effect of geological structure on microseismic disturbances*: *Mon. Not. Roy. Astr. Soc., Geoph. Suppl.*, v. 3, p. 83-105.
- Love, A. E. H., 1944, *A treatise on the mathematical theory of elasticity*: New York, Dover Publications.
- Northwood, T. D. and Anderson, D. V., 1953, *Model seismology*: *Bull. Seis. Soc. Am.*, v. 43, p. 239-246.
- Terada, T. and Tsuboi, C., 1927, *Experimental studies on elastic waves (Parts I and II)*: Tokyo Imperial University, *Bull. Earthquake Res. Inst.*, v. 3, p. 55-65, v. 4, p. 9-20.